Real-Space Tight-Binding LMTO Approach to Magnetic Anisotropy: Application to Nickel Films on Copper

D. Spišák and J. Hafner

Institut für Theoretische Physik and Center for Computational Materials Science, Technische Universität Wien, Wiedner Hauptstraße 8-10/136, A-1040 Vienna, Austria

Abstract. The basic ingredients of a real-space tight-binding linear-muffin-tin orbital (RS-TB-LMTO) approach to non-collinear magnetism and to torque-force calculations of the magnetic anisotropy are described. Applications to face-centered-tetragonal Ni films epitaxially grown on Cu(100) substrates are presented. The tetragonal distortion of the films is calculated using an *ab-initio* local-density technique, and the RS-TB-LMTO method is used for calculating the magnetic anisotropy in films with up to 7 Ni monolayers. The accuracy of the approach allows for a detailed analysis of second- and fourth-order anisotropy constants.

1 Introduction

The tight-binding linear muffin-tin orbital method [1] has proven to be a very efficient technique for investigating the electronic and magnetic properties of complex materials, both in its reciprocal- and real-space forms. Exemplary applications include disordered alloys [2,3], metallic glasses [4] and quasicrystalline alloys [5]. Of particular interest in the study of magnetism are systems where the magnetically ordered ground state cannot be described as a simple ferro-, antiferro-, or ferrimagnetic order with all moments aligned parallel or antiparallel to the global axis of magnetisation. In disordered systems the competition between ferro- and antiferromagnetic exchange interactions and/or fluctuating local anisotropies can lead to the formation of a non-collinear ground-state describable as a spin-glass, a spero-, speri-, or asperomagnet [6]. Non-collinear magnetic structures can also arise as a consequence of uncompensated magnetic interactions in ordered intermetallic compounds. The symmetry criteria for the formation of non-collinear spin structures have been discussed in Ref. [7].

Techniques for solving the Kohn–Sham equations of local-spin-density theory for a non-collinear magnet have been implemented in various standard electronic structure codes: the augmented spherical wave (ASW) method [8], the LMTO technique [9,10], and empirical tight-binding [11,12]. Applications include the helical magnetic structures of $\gamma-$Fe [9,13] and of YMn_2 [14], the non-collinear magnetism in Mn_3Sn [8], in metallic glasses [3], in quasicrystals [15] and in spin-glasses [2], to cite only a few examples.

The possibility to tilt the magnetic moment at a given site with respect to its equilibrium orientation opens the way to a calculation of Ising-, or Heisenberg-type exchange pair interactions, allowing even for a calculation of bilinear and

H. Dreyssé (Ed.): Workshop 1998, LNP 535, pp. 416–433, 1999.

biquadratic exchange couplings [16,17]. If spin-orbit coupling is included in the Hamiltonian, the magnetic anisotropy energy (MAE) can be calculated by a magnetic torque-force approach [18–20]. In both cases, the RS-TB-LMTO provides sufficient convergence whereas **k**-space calculations converge only when extremely fine grids are used for Brillouin-zone intergations [21,22]. In addition, they have the potential to make the underlying physical mechanism more transparent and to allow the investigation of even very complex systems.

In the present paper we first briefly review the fundamentals of the non-collinear spin-polarised RS-TB-LMTO technique and describe its application to the calculation of the magnetocrystalline anisotropy and to the exchange coupling constants. In the second part we present detailed investigations of the magnetic properties of the fcc Ni films epitaxially grown on Cu(001) surfaces. The Ni/Cu(001) system is unique because of the re-entrant character of the perpendicular magnetic anisotropy: with increasing film thickness, the magnetic anisotropy switches from in-plane to perpendicular at a thickness of about 7 monolayers, retaining the orientation of the magnetic moments normal to the film plane for a thickness of up to 60 **r**A [23,24]. In "normal" system the equilibrium between the spin-orbit driven anisotropy and the shape anisotropy leads to a single transition from perpendicular to in-plane with an increasing number of monolayers. It is believed that the re-entrant behaviour of Ni/Cu(001) films is largely strain-induced, driven by the lattice mismatch between film and substrate.

2 TB-LMTO Approach and Real-Space Recursion Formalism

Our approach to the self-consistent electronic-structure calculation is based on the two-center TB-LMTO Hamiltonian

$$H^{\alpha}_{ils,i'l's'} = \left[\frac{1}{2}\delta_{ii'}\delta_{ll'}(c^{\alpha}_{ils} + c^{\alpha}_{i'l's'}) + \sqrt{d^{\alpha}_{ils}}S^{\alpha}_{il,i'l'}\sqrt{d^{\alpha}_{i'l's'}}\right]\delta_{ss'} - \\ - \frac{1}{2}\delta_{ii'}\delta_{ll'}\Delta_{il}\sigma^{z}_{ss'} = H^{\alpha,\mathrm{para}}_{ils,i'l's'} + H^{\alpha,\mathrm{exch}}_{ils,i'l's'} \quad , \tag{1}$$

expressed in terms of the structure constants S^{α} and the potential parameters c^{α}, d^{α} which are evaluated in the screened most-localised representation [25]. The potential parameters depend on the solution of the radial Schrödinger equation at the energies ϵ_{ν} chosen usually at the center of the occupied part of the bands. Essentially, c^{α} describes the center of gravity of the bands whereas d^{α} measures the band width. The matrix element given by Eq. (1) refers to the interaction between atoms i, i', orbitals l, l' of the spin s, s'. The Pauli matrices will be denoted as σ^x, σ^y and σ^z.

The first term in of Eq. (1) describes the non-magnetic part of the band structure, the second spin-dependent term gives rise to the shifts of the bands with different spins in the opposite directions. The shift is controlled by the exchange splitting field

$$\Delta_{il} = c^{\alpha}_{il\downarrow} - c^{\alpha}_{il\uparrow} \quad . \tag{2}$$

Self-consistent calculations for various magnetic systems containing 3d- or 4d-metals reveal that the proportionality relation

$$\Delta_{il} = I_{il} m_{il} \quad , \tag{3}$$

between the exchange splitting field Δ_{il} and the magnetic moment m_{il} is satisfied very well for d-orbitals [4,26,27]. Therefore the non-selfconsistent studies based on the TB-LMTO formalism can use a fixed Stoner parameter of $I_2 = 0.95$ eV/μ_B as a very reasonable approximation.

Till now it was supposed that the magnetic moments are all aligned along the z axis. The generalization of the presented approach to the treatment of a non-collinear magnetic order consists in rewriting the exchange part of the Hamiltonian (1) to a rotation invariant form

$$H^{\alpha,\mathrm{exch}}_{ils,i'l's'} = -\frac{1}{2}\delta_{ii'}\delta_{ll'}\Delta_{il}\sigma_{ss'} = -\frac{1}{2}\delta_{ii'}\delta_{ll'} I_{il}\Delta_{il}\mathbf{n}_i.\sigma_{ss'} \quad , \tag{4}$$

where $\sigma = \sigma^x\ \mathbf{x} + \sigma^y\ \mathbf{y} + \sigma^z\ \mathbf{z}$ is the vector of the Pauli matrices with $\mathbf{x}$, $\mathbf{y}$, $\mathbf{z}$ the unit vectors spanning a global coordinate space and $\mathbf{n_i} = \mathbf{m_i}/|\mathbf{m_i}|$. Each magnetic moment direction defined by polar angles φ_i and ϑ_i with respect to the global coordinate system defines the moments' local coordinate system, in which the exchange part of the Hamiltonian keeps the form of Eq. (1) but with $\sigma^z = \sigma^z_i$ referring to the local coordinate system. Because the paramagnetic part of the Hamiltonian is constructed in the global coordinate system, the on-site exchange part must be transformed correspondingly for each atom. Of course, the opposite procedure of the transformation of the paramagnetic matrix elements, namely the structure constants into the local bases would be equivalent. Taking $\mathbf{n}_i = \cos\varphi_i \sin\vartheta_i\ \mathbf{x} + \sin\varphi_i \sin\vartheta_i\ \mathbf{y} + \cos\vartheta_i\ \mathbf{z}$ we obtain for the transformed exchange splitting field on the ith site

$$\begin{aligned} -\frac{1}{2} I_{il}\Delta_{il}\mathbf{n}_i\sigma &= -\frac{1}{2} I_{il}\Delta_{il} \begin{pmatrix} \cos\vartheta_i & \sin\vartheta_i \exp(-\mathrm{i}\varphi_i) \\ \sin\vartheta_i \exp(\mathrm{i}\varphi_i) & -\cos\vartheta_i \end{pmatrix} \\ &= -\frac{1}{2} I_{il}\Delta_{il} D(\varphi_i,\vartheta_i)\sigma^z_i D^{+}(\varphi_i,\vartheta_i) \quad . \end{aligned} \tag{5}$$

$D(\varphi_i,\vartheta_i)$ is the Wigner $s = \frac{1}{2}$ rotation matrix from the local coordination system to the global one

$$D(\varphi_i,\vartheta_i) = \begin{pmatrix} \cos\frac{\vartheta_i}{2}\exp\left(-\frac{\mathrm{i}}{2}\varphi_i\right) & -\sin\frac{\vartheta_i}{2}\exp\left(-\frac{\mathrm{i}}{2}\varphi_i\right) \\ \sin\frac{\vartheta_i}{2}\exp\left(\frac{\mathrm{i}}{2}\varphi_i\right) & \cos\frac{\vartheta_i}{2}\exp\left(\frac{\mathrm{i}}{2}\varphi_i\right) \end{pmatrix} . \tag{6}$$

The band-structure problem is solved using the real-space recursion method [28], which is very efficient in combination with the TB-LMTO Hamiltonian. Therefore complex systems with many degrees of freedom can be treated.

The determination of a non-collinear magnetic structure proceeds as follows. In the first step the ground state of the collinear magnetic arrangement is found for the Hamiltonian (1). The potential parameters c^α, d^α together with the Stoner parameters I_{i2} calculated from Eqs. (2) and (3) are used in the construction of the Hamiltonian for the non-collinear calculation with the exchange part due to Eq. (5), so that all the procedure is parameter-free. The starting magnetic moment vectors are distributed randomly or small random transversal components are added to the magnetic moments resulting from previous collinear calculation. Partial densities of states are obtained for the x-, y-, z-directions of a moment in its local basis by choosing as the starting recursion vector the normalized eigenvector of σ^x, σ^y, σ^z, respectively, for up and down spin directions. The starting recursion vector is then rotated to the global coordinate system by multiplying it with $D(\varphi_i, \vartheta_i)$ from Eq. (6). In general, the new magnetic moments obtained from the integrated projected densities of states will have transversal components with respect to the last moment directions. The partial densities of state along the direction of the magnetic moments are used in the update of the charge densities, potential parameters and exchange splitting fields at each step. The process continues in an iterative way until the transversal components are sufficiently small. The moment rotations are quite slow during the iteration process, therefore the new orientations are extrapolated from the old and new directions and besides random noise components are added in order to avoid running into nearest local minima. In the prediction of the new non-collinear structure we use a Broyden mixing scheme [29]. For further technical details of the non-collinear calculations we refer to the papers [10,19,30].

In some cases symmetry restrictions allow only a few special spin arrangements in a system. Then the aim is to find a ground state spin configuration. This kind of calculations can be done as described above but only the densities of state projected along the moments are necessary what results in the much faster calculation. To the group of models with fixed directions of magnetic moments belongs a determination of the magnetic anisotropy energy.

2.1 Magnetocrystalline Anisotropy

The spin-orbit coupling responsible for the magnetocrystalline anisotropy can be included into Hamiltonian given by Eq. (1) and Eq. (4) by adding an intra-atomic term

$$H^{\mathrm{so}}_{ils,i'l's'} = \frac{1}{2}\delta_{ll'}\xi_{ils,i'l's'}(E)\,(\sigma\mathbf{l})_{ils,i'l's'} \quad . \tag{7}$$

The matrix elements $\frac{1}{2}\,(\sigma\mathbf{l})_{ils,i'l's'}$ for the d-orbitals in the frame rotated to the magnetic moment direction can be found in Ref. [31]. The spin-orbit

Table 1. Spin-orbit coupling parameters in meV for iron, cobalt and nickel calculated at their experimental lattice constants for d-bands at the Fermi level E_F and at the middle of the occupied parts of the d-bands ϵ_ν. The results obtained by LSDA exchange-correlation potentials are compared with those obtained by GGA exchange-correlation potentials (in parentheses).

	$\xi_{d\uparrow}(E_F)$	$\xi_{d\downarrow}(E_F)$	$\xi_{d\uparrow}(\epsilon_\nu)$	$\xi_{d\downarrow}(\epsilon_\nu)$
Fe	72(72)	56(55)	58(58)	45(45)
Co	94(94)	78(78)	73(74)	63(63)
Ni	109(111)	103(103)	91(88)	84(84)

parameters $\xi_{ils,i'l's'}(E)$ are assumed to be non-negligible only between the d-orbitals centered on the same site and they are given in Ry units [32] as

$$\xi_{ils,i'ls'}(E) = \frac{2}{c^2}\delta_{ii'}\delta_{ll'}\int \phi_{ils}(E,r)\frac{dV(r)}{dr}\phi_{i'l's'}(E,r)r^2dr \quad . \tag{8}$$

Here c is the velocity of light, $\phi_{ils}(E,r)$ are the radial partial waves calculated at the energy E and $V(r)$ is the one-electron interaction potential. The spin-orbit coupling parameters obtained for iron, cobalt and nickel are shown in Table 1. We have found that using the Barth-Hedin-Janak local-spin-density approximation (LSDA) [33,34] and the generalised gradient approximation (GGA) [35] results for the spin-orbit coupling differing less than 3 %.

Because the spin-orbit coupling constants are much smaller than the band width for 3d-metals the magnetic anisotropy energy is often evaluated as a difference of the sums of the single-particle eigenvalues for the opposite spin directions treating the spin-orbit term (7) as a perturbation. Even then the calculations in the **k**-space are very laborious [21]. Recently it has been demonstrated in several papers that the real-space approach makes the task of the MAE estimation possible in a non-perturbative fashion from the total ground state energies [19,20,36]. From practical reasons the inclusion of the spin-orbit coupling in the non-collinear calculations has the advantage of reducing somewhat the drift of the overall magnetic moment in the course of the iteration process.

The determination of the preferential magnetisation orientation is of much interest especially for thin magnetic films and multilayers, which possess a lowered symmetry. However, in the layered systems the other significant contribution, the magnetostatic shape anisotropy coming from the dipole-dipole interaction, must be taken into account. Because the shape anisotropy always prefers the in-plane magnetisation, it is responsible for the changing the orientation of the magnetisation to the plane at some critical thickness if the spin-orbit contribution to the MAE happens to support a perpendicular anisotropy. When the thickness of the magnetic film is reduced to a few monolayers, the contributions from all discrete dipole pairs have to be summed up explicitly

$$E^{\mathrm{dip}} = \frac{1}{c^2} \sum_{<i,j>} \frac{1}{r_{ij}^3} \left(\mathbf{m}_i . \mathbf{m}_j - 3 \frac{\mathbf{m}_i . \mathbf{r}_{ij} \mathbf{m}_j . \mathbf{r}_{ij}}{r_{ij}^2} \right) \quad , \tag{9}$$

rather than to resort to the continuum approximation. The sums appearing in Eq. (9) converge slowly due to the long-range character of the dipole-dipole interaction but they can be efficiently evaluated in the reciprocal space [37]. For the cubic sc, bcc and fcc lattices with one atom type per layer the magnetostatic dipolar energy can be expressed in Ry units as

$$E^{\mathrm{dip}} = \frac{1}{c^2 a^3 n_{2D}^2} \sum_{<i,j>} m_i m_j (\cos\vartheta_i \cos\vartheta_j - \\ - \frac{1}{2} \cos(\varphi_i - \varphi_j) \sin\vartheta_i \sin\vartheta_j) M_{ij} \quad , \tag{10}$$

where n_{2D} means a number of atoms in one layer, a is the lattice parameter of the basic cubic cell and the M_{ij} are the dipolar Madelung constants tabulated in Table 2.

2.2 Exchange coupling constants

The modern spin-polarised band theory gives an accurate description of the magnetic ground state of most metals and alloys. The magnetic excitations from the ground state are described in terms of various spin models in which the strength of a pair interaction is controlled by a magnitude of the exchange coupling.

Recently we have derived expressions for the exchange pair coupling constants and some other related quantities within a real-space approach [16]. The exchange interaction between the ith and jth moments takes a form

$$J_{ij} = \frac{\Delta_i \Delta_j}{2\pi} \mathrm{Im} \int^{E_F} \mathrm{Tr}\; G_{ij}^{\uparrow\uparrow}(E) G_{ji}^{\downarrow\downarrow}(E) dE \quad , \tag{11}$$

Table 2. Dipolar Madelung constants for the sc, bcc and fcc lattice geometries provided the basic cubic cell of unit volume, z stands for the interlayer distance.

layer	z	sc	bcc	fcc
0	0	9.03362	9.03362	25.55094
1	$\frac{1}{2}$	—	4.17639	4.04301
2	1	-0.32746	-0.32746	-0.06402
3	$\frac{3}{2}$	—	0.01238	0.00072
4	2	-0.00055	-0.00055	0.00001

where Δ is the exchange splitting field defined by Eq. (2) and the off-site Green's functions $G_{ij}^{ss}(E)$ for the up and down spins are calculated by the recursion method using the bonding and antibonding combinations for the sites i and j.

The mean-field estimation of the Curie temperature is related to the on-site exchange coupling J_{ii} via

$$T_{C,i} = \frac{1}{3k_B}\left(\frac{1}{2}\Delta_i m_i - J_{ii}\right) \quad . \tag{12}$$

The critical temperature $T_{C,i}$ should be viewed as a measure of the local stability of the magnetic state of the ith atom surrounded by all other atoms.

Another quantity related to the exchange couplings and accessible to the experimental verification is the spin-wave stiffness constant

$$D_i = \sum_j J_{ij} r_{ij}^2 \quad . \tag{13}$$

Here r_{ij} are the lattice vectors. The results for the nearest and the next nearest exchange couplings, the Curie temperature and the stiffness constants for iron, cobalt and nickel are presented in Table 3. The stiffness constant for iron was calculated using the first 14 terms, for cobalt and for nickel the first 17 terms in Eq. (13) were taken into account. The overall agreement with the experimental data confirms that the spin models formulated originally for systems with localised magnetic moments can be still be used as a reasonable approximation for itinerant magnets.

3 Ni/Cu(001) Films

3.1 Atomic Structure

Recently we have witnessed extensive experimental [24,42–47] and theoretical investigations [48–50] of the Ni films grown on Cu. The Ni/(001)Cu system has an average lattice mismatch of only 2.6 % favoring a coherent growth of Ni on

Table 3. The nearest and the next nearest exchange couplings J_1, J_2, the experimental and the calculated values of Curie temperature T_C and the spin-wave stiffness constant D for iron, cobalt and nickel.

	J_1 (meV)	J_2 (meV)	T_C (K)	T_C^{exp} (K)	D (meV**r**A^2)	D^{exp} (meV**r**A^2)
Fe (bcc)	16.27	17.29	890	1044[a]	280	280[b]
Co (hcp)	25.05	4.11	1000	(β Co) 1388[c]	1900	580[b]
Ni (fcc)	4.62	0.20	290	627[a]	530	555[d]

[a] Ref. [38], [b] Ref. [39], [c] Ref. [40], [d] Ref. [41]

Table 4. The relaxed atomic structures of films with one to seven Ni layers on Cu(001) from first-principles calculations using the VASP package. The results are compared with the available experimental data taken at room temperature.

ML	1		2		3			5		7	fct Ni
d_{12}(%)	-6.2	-7.0	-11.9	-2.4	-11.4	-3.5	-1.1	-10.8	1.6	-11.0	-11.1
d_{23}(%)	0.2	-1.0	-1.9	-1.0	-7.4	-7.5	-3.9	-5.1	-6.1	-5.8	-6.2
d_{34}(%)			0.5	-0.5	-3.2	0.4	-2.8	-5.8	-5.0	-5.9	-6.9
d_{45}(%)					0.0	6.6	-1.1	-6.8	-5.6	-5.3	-7.0
d_{56}(%)								-1.2		-6.0	
d_{67}(%)								1.7		-6.2	
d_{78}(%)										-0.7	
d_{89}(%)										3.0	
Ref.		[45]		[45]		[45]	[46]		[46]		

Cu in an artificial tetragonally distorted face centered cubic (fct) structure up to a thickness of about 40 layers above which the growth continues in the fcc structure.

We investigated first the relaxation of films with one to seven Ni layers on Cu(001) using the spin-polarised version of the Vienna ab-initio simulation package (VASP). A detailed description of the VASP and its algorithms can be found in Ref. [51]. We used the Ceperley and Alder [52] local spin-density functional and the generalised gradient approximation corrections [35] to the exchange-correlation energy.

In the first step of the calculation the equilibrium lattice spacing of bulk Cu was found 3.637 **r**A, in close agreement with the measured value 3.61 **r**A. Then we performed a geometry optimisation of the Cu surface for a slab with 6 layers. We found a 3.6 % inward relaxation of the surface layer. The predicted relaxation agrees well with previous ab-initio calculations [53], but is somewhat lower than the relaxation found in experiment (1.2 % in Ref. [54], 2.4 % in Ref. [55]). The difference is mostly due to the fact that experiments have been performed at room temperature. Afterwards the slab was extended on one side with 1 to 7 Ni layers and during the relaxation the lateral lattice spacing was kept at the Cu bulk value. The inspection of the obtained layer relaxations summarised in Table 4 reveals clear trends. The surface layer undergoes a strong inward relaxation, the subsurface layers form a fct lattice with an axial ratio $c/a \approx 0.94$. The relaxation of the bulk fct Ni with the lattice spacing of the Cu bulk leads to a tetragonal distortion of $c/a \approx 0.93$. The rightmost column of Table 4 gives the structure of the fct Ni surface modeled as a slab of eight layers. Again the surface layer relaxes inward by a 11 % and the c/a ratio reaches the value 0.93 in the middle of the slab. The estimate within the continuum elasticity theory of coherent epitaxy-induced structural changes gives $c/a \approx 0.965$.

Table 5. Magnetic moments in relaxed Ni/Cu(001) films with up to seven monolayers of Ni and of fct Ni in μ_B. First two interface Cu layers are shown as well. The results within RS-TB-LMTO approach can be compared with the moments obtained by VASP package (right columns).

ML	1		2		3		5		7		fct Ni	
1	0.12	0.38	0.76	0.75	0.78	0.74	0.77	0.74	0.74	0.73		
2	0.00	0.01	0.48	0.52	0.55	0.59	0.58	0.68	0.58	0.68		
3	-0.00	-0.01	-0.01	-0.01	0.50	0.47	0.69	0.71	0.68	0.69		
4			-0.00	0.00	-0.01	0.00	0.62	0.69	0.64	0.68		
5					-0.01	0.00	0.48	0.58	0.68	0.71		
6							-0.01	0.01	0.64	0.70		
7							-0.01	0.00	0.47	0.58		
8									-0.01	-0.01		
9									-0.01	-0.01		
$\bar{m}$	0.12	0.38	0.62	0.63	0.61	0.60	0.63	0.68	0.63	0.68	0.66	0.61

For a single monolayer of Ni/Cu(001), the predicted relaxation is in very good agreement with low-energy electron-diffraction (LEED) experiments by Kim et al. [45]. For thicker layers, however, LEED experiments predict only a minimal inward relaxation (and for yet thicker layers even an outward relaxation) of the top layer [45,46], at an almost homogeneous tetragonal distortion of the deeper part of the film. The first-principle calculations, on the other side predict a large inward relaxation ot the toplayer, but agree with experiment concerning the tetragonal distortion of the interior of the film.

Recent ab-initio calculations (based on the same technique) of the structural, electronic and magnetic properties of all low index surfaces of Ni [56] lead to excellent agreement with experiment. Similar discrepancies between ab-initio calculation and the experiment as those observed for Ni/Cu(001) have been recorded for a number of transition metal surfaces, e.g. Rh(001) and attributed to an anomalously large perpendicular thermal expansion at the surface [57], limiting the comparison between the room-temperature experiment and the T = 0 K calculation. It must be left to the future work whether this mechanism also explains the discrepancy between calculations and experiment for the surface of Ni/Cu(001) films.

3.2 Magnetic Structure

Using the relaxed atomic structural models discussed in the previous paragraph we have calculated the magnetic structure and the magnetic anisotropy energy

Table 6. Spin-orbit coupling parameters for up (left columns) and down (right columns) partial waves in the relaxed Ni/Cu(001) films with up to seven layers of Ni in meV. The results for bulk fct Ni are shown in the right-most column.

ML	1		2		3		5		7		fct Ni	
1	97.3	95.9	107.2	98.3	106.8	97.7	106.6	97.6	106.5	97.8		
2			105.7	102.6	111.6	104.5	111.3	103.8	111.8	104.3		
3					107.1	101.0	111.1	102.3	111.4	102.7		
4							110.8	102.9	110.7	102.6		
5							106.6	100.7	111.3	102.7		
6									111.4	103.2		
7									106.7	100.7		
											110.2	101.9

of the Ni/Cu(001) films within the framework of RS-TB-LMTO method. The real-space recursion technique was applied to cells with 1944 atoms for 1 Ni monolayer (ML) up to 2560 atoms for 7 Ni ML. Periodic boundary conditions in the lateral directions and the free boundary conditions normal to the layers were used. In all cases 20, 20, and 50 recursion levels were used for the s-, p-, d-orbitals, respectively. Because for the thicker Ni films we obtained a systematic inward relaxation 6 %, we studied also an infinite fct Ni crystal with the tetragonal distortion $c/a = 0.94$.

The layer-resolved and the average magnetic moments are shown in Table 5. As can be expected, the moments at the surface are enhanced (except for the monolayer) while the moments at the interface drop. This behaviour is observed independent of the film thickness. Although the total average magnetic moment approaches the bulk value gradually, even the system with 7 Ni ML is influenced so strongly by the surface that it is not possible to identify a subsurface region with steady bulk-like magnetic moments. We also note that the RS-TB-LMTO calculations agree well with **k**-space results obtained using VASP.

Due to the relatively low Curie temperature of bulk Ni, the thin films of Ni can be studied in a wide temperature range as a function of film thickness. The comprehensive collection of experimental data establishes a clear picture of magnetic anisotropies in Ni/Cu(001) films [24,43,44]. As the film thickness increases the magnetisation changes its direction from [100] to [110] between 6 and 7 Ni ML and between 7 and 8 Ni ML it switches continuously to the [001] direction. The surface and volume contributions to the second-order anisotropy constants K_2^s and K_2^v at zero temperature lie between -100 up to -180 μeV/atom and 40 up to 75 μeV/atom [44], respectively. The large error bars are due to the uncertainty in the extrapolation down to zero temperature. For the fourth-order in-plane and out-of-plane anisotropy constants very small values of $K_{4\|} \approx$

-1 μeV/atom and $K_{4\perp} \approx 0.2$ μeV/atom at $T/T_c = 0.8$ were reported for 7 Ni ML [44].

We calculated MAE using the force theorem [21], treating the spin-orbit coupling as a perturbation. As can be seen from Table 6 the spin-orbit coupling parameters are only slightly affected by the surface and interface. The layer-resolved and the total band and dipole-dipole contributions to the MAE are compiled in Table 7. The contributions of the surface layer to the MAE in all but monolayer films support an out-of-plane orientation of the magnetisation and the magnitude of these contributions saturates with the film thickness. The contribution of the Ni layer at the interface to the Cu substrate also prefers a perpendicular orientation of the magnetic moments (except for the 2 ML film), but does not show a systematic variation as the number of layers increases. Quite surprisingly, we also find a large contribution from the subsurface layer and the second Ni layer from interface, always preferring an in-plane orientation. The contributions from the inner layers in films with ≥ 5 ML are always smaller than the surface and interface contributions. As can be seen from Fig. 1, the 2 ML and 3 ML films show the perpendicular magnetic anisotropy, all other films we have investigated have an easy axis in the plane. The spin-reorientation transition between the 3 ML and 5 ML case is driven by the subsurface contribution to the MAE. For the Ni monolayer we predict $K_2 = -263$ μeV/atom in a fair agreement with the measured value about -157 μeV/atom [43], previous calculations giving -94 μeV/atom [48] or -690 μeV/atom [50]. For 2 Ni ML our result $K_2 =$

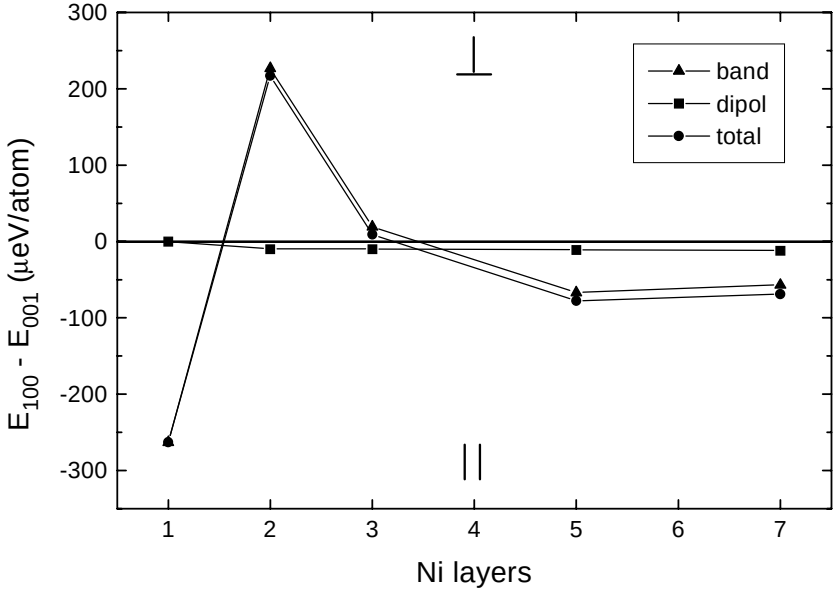

Fig. 1. Calcutated total magnetic anisotropy energy (circles) and its dipole-dipole (triangles) and band (squares) contributions for thin Ni films on Cu(001).

Table 7. Spin-orbit ($\triangle E_{\rm b}$, left columns) and dipolar ($\triangle E_{\rm d}$, right columns) contributions to the magnetic anisotropy energy $\triangle E = E_{100} - E_{001}$ in the relaxed Ni/Cu(001) films with up to seven Ni layers. In the last row the estimate of the fourth-order anisotropy constant $K_{4\parallel} = 4(E_{110} - E_{100})$ is given. The values for the layer-resolved contributions are in μeV, the averaged values are in μeV/atom.

ML	1		2		3		5		7		fct Ni	
1	-263	0	822	-14	1511	-15	2046	-15	2202	-14		
2			-369	-7	-2112	-10	-1036	-11	-1049	-11		
3					659	-6	355	-14	254	-13		
4							-1870	-11	-641	-12		
5							168	-6	-316	-13		
6									-1330	-12		
7									481	-6		
$\triangle \bar{E}_{\rm b,d}$	-263	0	227	-10	19	-10	-67	-11	-57	-12	52	0
$\triangle(\bar{E}_{\rm b} + \bar{E}_{\rm d})$	-263		217		9		-78		-69		52	
$K_{4\parallel}$	-331		103		24		-17		-6		-3	

227 μeV/atom compares very well with $K_2 = 300$ μeV/atom obtained by Wu and Freeman [50]. We note that the earlier calculations considered unrelaxed fct or fcc lattices.

For an infinite fct Ni crystal with the tetragonal distortion $c/a = 0.94$ we performed a series of calculations for models with different number of atoms. We obtained almost the same values for the MAE 50, 54, 52 μeV/atom for cells with 2048, 2916 and 6912 atoms, respectively. These values are only a bit lower than results 60 μeV [49] and 65 μeV [50] found in the **k**-space calculations.

The decreasing negative values of the MAE for 5 and 7 ML, together with the positive value for the infinite fct Ni indicate the possibility of an in-plane to perpendicular reorientation at a thickness > 7 ML. However, it must be left to future studies to locate this transition precisely.

The MAE for 2 Ni ML as a function of the tilt angle ϑ taken from the [001] direction is shown in Fig 2. The dependence on $\cos^2\vartheta$ is almost linear. Our attempt to estimate the higher-order term yields a ratio between the fourth-order and the second-order contribution of 0.01. Here and below we use for the angular dependence of the MAE the expression [44]

$$E(\varphi,\vartheta) = E_0 - K_2\cos^2\vartheta - \frac{1}{2}K_{4\perp}\cos^4\vartheta - \frac{1}{8}K_{4\parallel}(3+\cos 4\varphi)\sin^4\vartheta \quad . \qquad (14)$$

Whether the reorientation of the magnetisation between the in-plane and out-of-plane orientations happens continuously or abruptly depends on the sign of

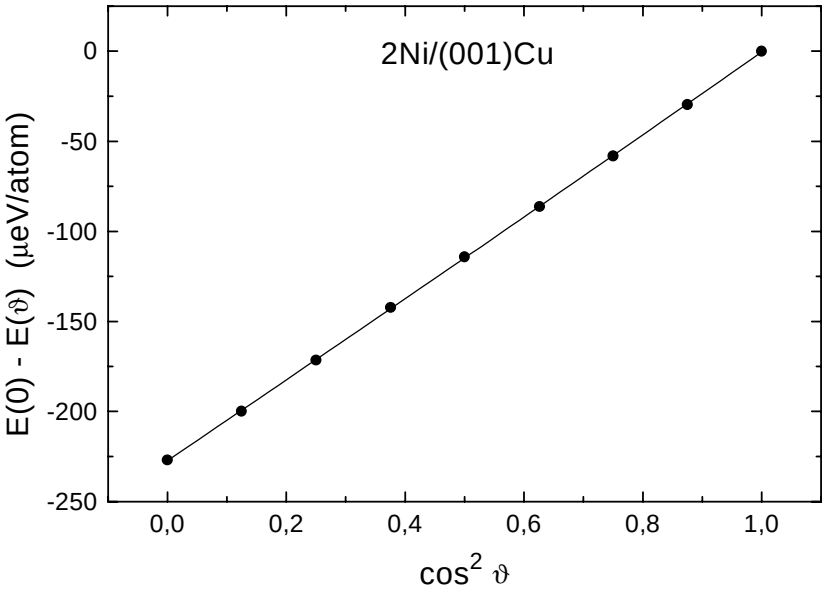

Fig. 2. Band energy difference plotted as a function of ϑ for 2 Ni ML films on Cu(001). The solid line represents the fit by a parabola.

$K_{4\|}$. For a stabilisation of a tilted magnetisation (and hence a continuous second or higher order spin-reorientation transition) a negative $K_{4\|}$ is needed. The value of the fourth-order in-plane anisotropy constant $K_{4\|}$ can be obtained from the variation of the MAE with $\cos 4\varphi$. In the last row of Table 7 we show our results for $K_{4\|}$. It can be concluded that its thickness dependence is rather complex and the $K_{4\|}$ changes sign between 3 and 5 ML. Because these values are typically as small as few μeV we carried out additional calculations for several intermediate angles between 0 and 45° for 2, 3 and 7 ML films (Fig. 3). From the scatter of the points around a linear fit versus $\cos 4\varphi$ we estimate that the confidence level in the numerical accuracy of our approach is better than 0.3 μeV/atom in all cases. Actually, the curves for 2 and 3 ML seem to be modulated systematically. Despite of the exceedingly small values of the fourth-order MAE the calculated values are in a reasonable agreement with experimentally observed trends.

In order to understand the influence of the surface and of the tetragonal distortion of the films on the magnetic anisotropy, a correlation between the number of holes in the Ni-d band (as observable in near-edge x-ray-absorption fine-structure (NEXAFS) experiments) and possible anisotropy of the d-band occupation has been evoked [47]. It has been argued that the number of holes in the Ni-d band is strongly reduced in the thinnest films, converging to a bulk-like value at a thickness of about 5 ML. In addition, an in-plane character of the d-holes irrespective of the thickness has been reported.

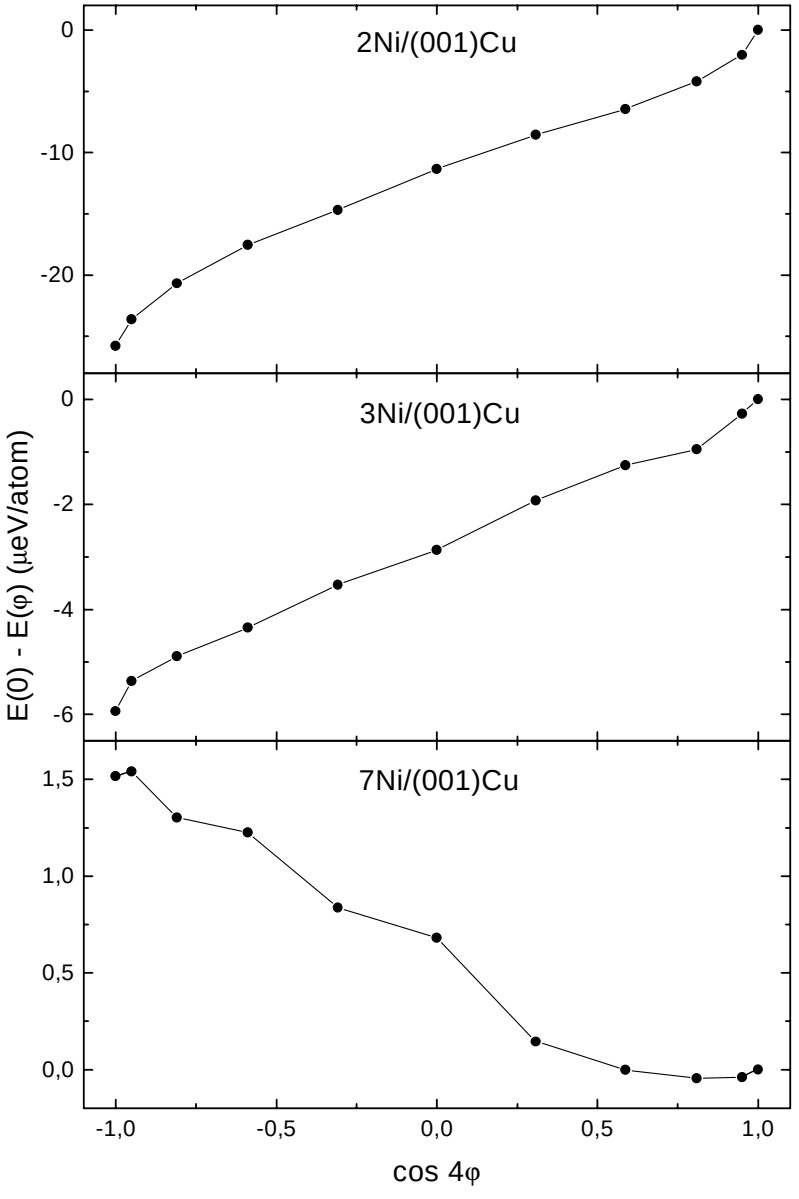

Fig. 3. Band energy difference plotted as a function of φ for 2, 3 and 7 Ni ML films on Cu(001).

In Table 8 we present the number of 3d-holes (unoccupied states) separated into holes in in-plane orbitals (xy, $x^2 - y^2$ for the (001) plane) and out-of-plane orbitals (yz, zx and $3z^2 - r^2$ for the (001) plane). It is obvious that the 3d-

Table 8. Numbers of 3d-holes with the in-plane ($d_\parallel$, left columns) and out-of-plane ($d_\perp$, right columns) symmetry for Ni atoms in one to seven Ni/Cu(001) films. The ratio $\bar{d}_\parallel/\bar{d}_\perp$ determines the character of the holes ($\bar{d}_\parallel/\bar{d}_\perp > 2/3$ means in-plane character, $\bar{d}_\parallel/\bar{d}_\perp < 2/3$ means out-of-plane character). The results for bulk fct Ni are shown in the rightmost column.

ML	1		2		3		5		7		fct Ni	
1	0.73	0.62	0.70	0.74	0.67	0.77	0.68	0.76	0.66	0.78		
2			0.53	0.88	0.51	0.93	0.51	0.93	0.51	0.93		
5					0.59	0.86	0.56	0.92	0.56	0.93		
6							0.55	0.92	0.56	0.92		
7							0.58	0.85	0.56	0.92		
									0.54	0.94		
									0.57	0.86		
$\bar{d}_{\parallel,\perp}$	0.73	0.62	0.61	0.81	0.59	0.85	0.58	0.88	0.57	0.90	0.55	0.91
$\bar{d}_\parallel + \bar{d}_\perp$	1.35		1.42		1.44		1.45		1.46		1.46	
$\bar{d}_\parallel/\bar{d}_\perp$	1.17		0.76		0.69		0.66		0.63		0.61	

band filling is reduced progressively as the film thickness increases and at the same time the hole character changes from the in-plane to out-of-plane between 4 and 5 Ni ML. The increase of the number of Ni holes with increasing film thickness compares well with the experimental observations reported in Ref. [47]. In addition we find that the ratio $d_\parallel/d_\perp$ is enhanced in the surface layer over the value $d_\parallel/d_\perp = 2/3$ corresponding to an isotropic distribution of the 3d-holes. Again this agrees with the conclusions derived from the NEXAFS experiments where the anisotropy has been attributed to the tetragonal distortion of the films. However, whether this conjecture is correct remains to be verified by reference calculations for undistorted films. The in-plane character of the 3d-holes means at the same time that the 3d-electrons have perpendicular character, and this agrees with the positive contributions of the surface layers to the MAE. In the deeper layers, the ratio $d_\parallel/d_\perp$ drops below 2/3 and is smallest in the subsurface layer and the second layer from the interface. Again this correlates well with the negative contributions to the MAE noted for these layers. Taking the average over the entire film, we find that the hole character changes between 3 and 5 ML what correlates with the reversal of the MAE. Altogether this analysis demonstrates that there are important changes in the partial electronic density of states near the Fermi level as a function of the film thickness whose evident correlations to the MAE deserve further investigation.

4 Conclusions

The RS-TB-LMTO formalism described in the first part of the paper, together with an *ab-initio* density functional approach to the reconstruction of the films, has been applied to study the variation of the magnetic anisotropy of Ni/Cu(001) films with increasing film thickness. The predicted tetragonal distortion of the deeper layers agrees with experimental observations, but there is disagreement concerning the obtained inward relaxation of the top layer – this is possibly related to the confrontation of the T = 0 K calculations with room-temperature experiments.

For the magnetic anisotropy, we predict a very complex behaviour: the change from in-plane (1 ML) to perpendicular (2, 3 ML) back to in-plane(5, 7 ML) and eventually again back to perpendicular for thicker layers (as long as the film remains tetragonally distorted). A detailed analysis reveals a competition between surface and interface contributions favouring a perpendicular orientation and subsurface and subinterface contributions favouring in-plane orientation of the magnetic moments. The correlations to a changing anisotropic population of the Ni-3d bands have been investigated and found to agree with the interpretation of NEXAFS experiments.

Acknowledgments

This work has been supported by the Austrian Ministery for Science and Transport within the project "Magnetism on the Nanometer Scale".

References

1. Andersen, O. K., Jepsen, O., Šob, M. in: Electronic Band Structure and its Applications, Ed. Yussouff, M., Springer, Berlin (1986).
2. Becker, Ch., Hafner, J., Lorenz, R. , J. Magn. Magn. Mat. **157-158**, 619 (1996).
3. Lorenz, R., Hafner, J., Jaswal, S. S., Sellmyer, D., J., Phys. Rev. Lett. **74**, 3688 (1995).
4. Turek, I., Becker, Ch., Hafner, J., J. Phys.: Condens. Matter **4**, 7257 (1992).
5. Hafner, J., Krajči, M., Phys. Rev. B **57**, 2849 (1998).
6. Mattis, D., C., The Theory of Magnetism, Vols. I-II, Springer, Berlin (1985).
7. Sandratskii, L., M. , Adv. Phys **47**, 91 (1985).
8. Sticht, J., Höck, K.-H., Kübler, J. , J. Phys.: Condens. Matter **1**, 8155 (1989).
9. Mryasov, O. N., Liechtenstein, A. I., Sandratskii, L. M., Gubanov, V. A. J. Phys.: Condens. Matter **3**, 7683 (1991).
10. Lorenz, R., Hafner, J., J. Magn. Magn. Mat. **139**, 209 (1995).
11. Krey, U., Krompiewski, S., Krauss, U., J. Magn. Magn. Mat. **86**, 85 (1990).
12. Freyss M., Stoeffler, D., Dreyssé, H., , Phys. Rev. B **54**, R12677 (1996).
13. Uhl, M., Sandratskii, L., M., Kübler, J., J. Magn. Magn. Mat. **103**, 314 (1992).
14. Kübler, J., Sandratskii, L. M., Uhl, M., J. Magn. Magn. Mat. **104-107**, 695 (1992).
15. Smirnov, A., V., Bratkovsky, A., M., Phys. Rev. B **53**, 8515 (1996).
16. Spišák, D., Hafner, J., J. Magn. Magn. Mat. **168**, 257 (1997).

17. Spišák, D., Hafner, J., Phys. Rev. B **55** 8304 (1997), ibid. B **56**, 2646 (1997).
18. Lorenz, R., Hafner, J., J. Phys.: Condens. Matter **7**, L253 (1995).
19. Lorenz, R., Hafner, J., Phys. Rev. B **54**, 15 937 (1996).
20. Beiden, S. V., Temmerman, W., M., Szotek, Z., Gehring, G. A., Stocks, G., M., Wang, Y., Nicholson, D. M. C., Shelton,W. A., Ebert, H., Phys. Rev. B **57**, 14 247 (1998).
21. Daalderop, G. H. O., Kelly, P. J., Schuurmans, M. F. H., Phys. Rev. B **41**, 11919 (1990).
22. Hoermandinger, G., Weinberger, P. ,J. Phys.: Condens. Matter **4**, 2185(1992) .
23. Schulz, B., Baberschke, K., Phys. Rev. B **50**, 13 467 (1994).
24. Bochi, G., Ballentine, C. A., Inglefield, H. E., Thompson, C. V., O'Handley, R. C., Hug Hans J., Stiefel, B., Moser, A., Güntherodt, H.-J., Phys. Rev. B **52**, 7311 (1995).
25. Nowak, H. J., Andersen, O. K., Fujiwara, T., Jepsen, O., P. Vargas, P., Phys. Rev. B **44**, 3577 (1991) .
26. Becker, Ch., Hafner, J., Phys. Rev. B **50**, 3933 (1994).
27. Spišák, D., Becker, Ch., Hafner, J., Phys. Rev. B **51**, 11 616 (1995).
28. Haydock, R., Heine, V., Kelly, M. J. in: Solid State Physics, Advances in Research and Applications, Eds. Ehrenreich, H., Turnbull, D., Seitz, F., Vol **35** Academic Press, New York (1980).
29. Srivastava, G. P., J. Phys. A: Math. Gen. **17**, L317 (1984).
30. Lorenz, R., Hafner, J., Phys. Rev. B **58**, 5197 (1998).
31. Abate, E., Asdente, M., Phys. Rev. **140**, A1303 (1965).
32. Andersen, O. K., Phys. Rev. B **12**, 3060 (1975).
33. von Barth, U., Hedin, L. , J. Phys. C: Solid State Phys. **5**, 1629 (1972).
34. Janak, J. F., Solid State Commun. **25**, 53 (1978).
35. Perdew, J. P., Wang, Y., Phys. Rev. B **45**, 13 244 (1992). **41**, 11 919
36. Dorantes-Dávila, J., Pastor, G. M., Phys. Rev. Lett. **77**, 4450 (1996).
37. Tsymbal, E., J. Magn. Magn. Mat. **130**, L6 (1994).
38. Leger, J. M., Loriers-Susse, C., Vodar, B., Phys. Rev. B **6**, 4250 (1972).
39. Panthenet, R., J. Appl. Phys. **53**, 8187 (1982).
40. Cowan, D. L., Anderson, L. W., Phys. Rev. A **139**, 424 (1965).
41. Mook, H. A., Lynn, J. W., Nicklow, R. M., Phys. Rev. Lett. **30**, 556 (1973).
42. Huang, F., Kief, M. T., Mankey, G. J., Willis, R. F., Phys. Rev. B **49**, 3962 (1994).
43. Baberschke, K., Appl. Phys. A **62**, 417 (1996).
44. Farle, M., Mirwald-Schulz, B., Anisimov, A. N., Platow, W., Baberschke, K., Phys. Rev. B **55**, 3708 (1997).
45. Kim, S. H., Lee, K. S., Min, H. G., Seo, J., Hong, S. C., Rho, T. H., Kim, J.-S., Phys. Rev. B **55**, 7904 (1997).
46. Müller, S., Schulz, B., Kostka, G., Farle, M., Heinz, K., Baberschke, K., Surf. Science **364**, 235 (1996).
47. Srivastava, P., Haack, N., Wende, H., Chauvistré, R., Baberschke, K., Phys. Rev. B **56**, R4398 (1997).
48. Moos, T. H., Hübner, W., Bennemann, K. H., Solid State Commun. **98**, 639 (1996).
49. Hjortstam, O., Baberschke, K., Wills, J. M., Johansson, B., Eriksson, O., Phys. Rev. B **55**, 15026 (1997).
50. Wu, R., Chen, L., Freeman, A. J., J. Appl. Phys.**81**, 4417 (1997).
51. Kresse, G., Furthmüller, J., Comput. Mater. Sci. **6**, 15 (1996), Phys. Rev. B **54**, 11 169 (1996).
52. Ceperley D. M., Alder, B. J., Phys. Rev. Lett. **45**, 566 (1980).

53. Rodach, Th., Bohnen, K.-P., Ho, K. M., Surf. Sci. **286**, 66 (1993).
54. Lind, D., M., Dunning, F., B., Walters, G. K., Davis, H. L., Phys. Rev. B **35**, 9037 (1987).
55. Jiang, Q., T., Fenter, P., Gustafsson, T. Phys. Rev. B **44**, 5773 (1991).
56. Mittendorfer, F., Eichler, A., Hafner, J., Surf. Sci. (in press) (1998).
57. Cho, J. H., Scheffler, M., Phys. Rev. Lett. **78**, 1299 (1997).